Research Article | Vol. 11, No. 8 / 1 August 2021 / Optical Materials Express 2712

Optical Materials EXPRESS

Highly reflective visible color filter based on a double layer TiO_2 subwavelength structure

YUUSUKE TAKASHIMA,[1,2,*] MASANOBU HARAGUCHI,[1,2] AND YOSHIKI NAOI[1,2]

[1] *Graduate School of Technology, Industrial and Social Sciences, Tokushima University, Tokushima 770-8506, Japan*
[2] *Institute of Post-LED Photonics, Tokushima University, Tokushima 770-8506, Japan*
[*] *takashima@tokushima-u.ac.jp*

Abstract: Color filters based on all-dielectric subwavelength structures (SWSs) allow precise control of the coloration during production. However, SWS manufacturing typically requires complex processes, such as lift-off or etching. Here, highly reflective color filters manufactured without lift-off and etching techniques were experimentally demonstrated using a double-layer high-contrast all-dielectric SWS. The SWSs were fabricated on optical glass substrates using electron beam lithography and evaporation. Visible reflection spectra were controlled by adjusting structural parameters. Red, green, and blue colorations were experimentally demonstrated with 57%, 63%, and 72% reflectivities, respectively. High reflectivity, manufacturing throughput and level of control of the manufactured filter color make them suitable for imaging, display, and sensing applications.

1. Introduction

Color filters, which transmit, reflect, or absorb a certain wavelength in the visible light region, are essential for applications such as imaging and displays [1]. In particular, the practical applications of these filters require exact filter colors, high efficiency, and high throughput. Traditional color filters are composed of several pigments and dyes. Their performance, such as operating wavelengths, bandwidth, and efficiency, is restricted by the light absorption characteristics of the pigments and dyes that the filters are composed of.

Structural color-based filters with subwavelength structures (SWSs) have several advantages over conventional filters because one can arbitrarily control optical characteristics by adjusting structural dimensions of the SWSs. Surface plasmon resonances (SPRs) in nanostructured metal films [2], metal nano slits [3], two-dimensional (2D) metal structure arrays [4], and nanowires [5] have been widely employed for high spectral resolution color filters. Plasmonic structures have achieved unique and attractive applications, such as polarization-switching dual color filters [2], active color filters [6], and sub-diffraction limited optical imaging [7]. Several groups reported structural color filters with metal subwavelength grating on dielectric waveguides [8] and on etalon [9] to improve efficiency of the filters. However, these metal-composed color filters still suffer from intrinsic ohm loss of the metals.

Alternatively, all dielectric SWSs with high contrast of refractive index (RI) have attracted much research interest owing to the possibility to avoid the ohm loss in the metals. Many types of all-dielectric SWS-based filters have been reported, such as nano blocks [10,11], cylinders [12–14], gratings [15,16], and cross-shaped resonators [17]; these dielectric-based SWSs have simultaneously achieved high-efficiency and high-color-selectivity. The SWSs were generally manufactured using lift-off or etching processes. These fabrication processes are laborious for subwavelength structural dimensions (generally 100 ~ 500 nm in visible region), and the collapse of SWS patterns often occurs. This is a critical obstacle for high manufacturing throughput of

#433431 https://doi.org/10.1364/OME.433431
Journal © 2021 Received 8 Jun 2021; revised 20 Jul 2021; accepted 20 Jul 2021; published 27 Jul 2021

Optical Materials EXPRESS

the color filters. For practical use of SWS color filters, there is a need for high-efficiency color filters that can be fabricated without lift-off and etching processes.

In this study, we experimentally demonstrated highly reflective color filters, including red (R), green (G), and blue (B), using double-layer dielectric SWSs manufactured without the etching and lift-off processes. The double-layer SWSs with structural parameters were fabricated with only electron beam (EB) lithography and evaporation techniques. The reflected light from the fabricated filters shows good control of the filter color and high efficiency in the visible wavelength region.

2. Design of double-layer SWS

Figure 1 depicts the schematic of the proposed double-layer SWS based color filter. As shown in Fig. 1(a) and 1(b), double-layer high RI materials are arranged with subwavelength period Λ on the low RI substrate. The width of the lower high RI material is w_1. The widths of the upper high RI materials and spacer materials are represented as w_2. The filling factor *(FF)* is defined as w_1/Λ. The thicknesses of the upper and lower high RI materials are represented as t. The upper and lower high RI materials are separated by the spacer composed of low RI material, and the distance between these is d. The SWS is surrounded by air.

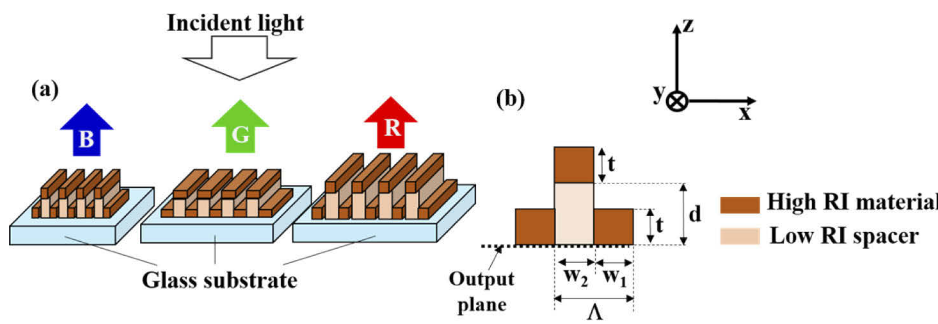

Fig. 1. (a) Schematic of double-layer high-contrast SWS-based color filter. (b) One cell of the double-layer SWS. Dark and light browns represent the high refractive index (RI) material and low RI spacer, respectively.

Here, we consider the normal incidence of the plane wave from the air side, as shown in Fig. 1(a). In the double-layer SWS, the eigenmodes are excited owing to the periodic RI distribution of each upper and lower SWS [18–20]. The phase of the modes can be significantly varied by structural parameters of SWSs because the phases depend on the structural dimensions of not only the lower SWS but also the upper one. This allows wider control of the optical characteristics of the double-layer SWS by adjusting the structural parameters, compared with a single SWS. Moreover, the lift-off and etching processes are not necessary for fabrication of the double-layer SWS, and it can be formed by lithography and deposition processes only. The ease of fabrication significantly contributes to improvement of throughput, and the fabrication method has good compatibility for mass production processes, such as nano-imprinting.

We explained the color generation in our proposed double-layer SWS. Outside the SWS, only 0th transmitted and reflected diffractions are propagative owing to its shorter period than the incident wavelength, and other orders are of evanescent form [20,21]. Inside the SWS, the high and abrupt RI contrast of the SWS supports several order eigenmodes. The excited modes accumulate a different phase after the propagation along the upper and lower SWSs. At the output plane in Fig. 1(b), the modes are not only reflected but also mixed to each other owing to its high contrast RI of SWS. As a result, the transmitted coefficient of 0th order diffraction τ_0 are given as

Optical Materials EXPRESS

following equation due to continuity of the electromagnetic field [20].

$$\tau_0 \propto \sum\nolimits_m (a_m + a_m^{\rho})\Lambda^{-1} \int_0^{\Lambda} e_{x,m}^{in}(x)dx \tag{1}$$

Here, m, a_m, and $a^{\rho}{}_m$ are orders of the excited modes, and the amplitudes of forward (-z) and backward (+z) propagating modes, respectively. The symbol $e_{x,\ m}{}^{in}$ (x) is the lateral (x-direction) electric field profile of the eigenmode at the output plane. According to Eq. (1), the transmitted light (0th diffraction) through the SWS strongly depends on the lateral (x-direction) field average of the eigenmodes. When the structural dimensions of the SWS are carefully selected to vanish the average of the lateral field at the output plane, the incident light energy is fully reflected back to the incident region at a certain wavelength (resonance wavelength). On the other hand, most of the incident energy passes through the SWS at non-resonance wavelength. Thus, high-efficiency arbitrary color generation can be realized. In addition, the 1-dimensional structures are polarization-sensitive [19,20], which provides unique applications, such as polarization-tunable color and bandwidth tuning [2,22,23].

Based on the SWS design rule mentioned before, the structural parameters of three samples (labeled as A, B, and C) were carefully chosen to generate various colors with high efficiency. We selected TiO_2 as high RI material due to its high RI value (typically, about 2.1 ~ 2.2) and its transparency in the visible wavelength region [24]. The spacer and the substrate were EB resist (ZEP-520A: Zeon Co.) and commercialized glass (D 263 T eco Thin Glass: SCHOTT Co.). The structural parameters of the designed samples are listed in Table 1. The filling factor and spacer thickness of each of the samples were fixed to $FF = 0.5$ and $d = 100$ nm, respectively.

Table 1. Dimensions of each designed SWS

Sample	A	B	C
Λ [nm]	250	300	400
FF (w_1/Λ)	0.5	0.5	0.5
d [nm]	100	100	100
t [nm]	80	120	150

To estimate the optical performance of our double-layer SWSs, the electromagnetic field distributions of the designed structures for p-polarized light (electric field perpendicular to the SWS fingers) were calculated by the 2D finite-difference time-domain (FDTD) method (Fullwave: R-Soft Co.). Figure 2 shows the calculation model of the double-layer SWS. In the 2D FDTD calculation, the double-layer TiO_2-SWS was placed on the optical glass substrate. The surrounding material was air (RI value = 1). The lengths of these objects were assumed to be infinite along the y-direction. The green square depicts the boundary conditions. The z-direction boundaries were perfectly matched layers (PMLs). No reflection appeared at the surface of the PMLs, and the intensity of the light inside the PMLs was significantly attenuated. Hence, the model assumed that the glass substrate was infinitely thick. The periodic boundary conditions (PBCs) were applied for the x-direction, and the electromagnetic field distribution was infinitely repeated for the x-direction. The p-polarized plane wave propagating along the z-direction vertically enters from the air side to the double-layer SWS. The reflected light intensity was calculated by the Poynting vector. For the calculations to converge, the spatial grids and incremental time of the FDTD calculation were set to 2 nm and 4.7×10^{-12} s, respectively.

Figure 3 shows the calculated reflection spectra of our designed samples A, B, and C. In the calculated spectra, the reflection peaks at different resonant wavelengths are obtained for each sample. The peak wavelengths of samples A, B, and C are 406 nm, 497 nm, and 647 nm, respectively. The values of the peak reflectivity reached nearly 100%. In order to reveal the origin of the resonant reflection peaks, Fig. 4(a) and 4(b) also present the calculated electric

Optical Materials EXPRESS

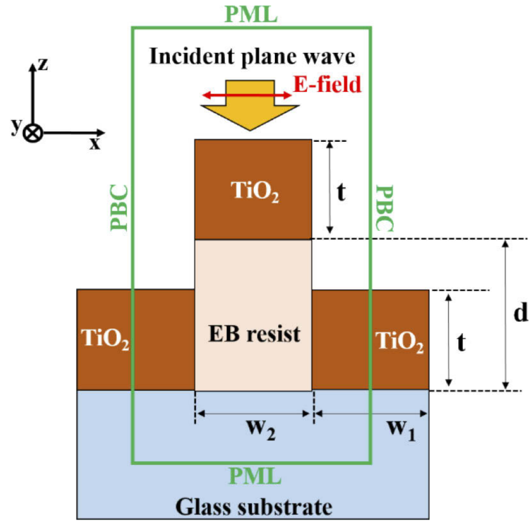

Fig. 2. FDTD calculation model of the double-layer SWS.

field distributions of sample A at a non-resonant (500 nm) and resonant wavelength (406 nm), respectively. As shown in Fig. 4(a), the amplitudes of the fields in the EB resist and lower TiO_2 are in-phase at the non-resonant wavelength. As a result, the field average at the boundary between the double-layer SWS and the glass substrate is large, and most of the incident energy is transmitted through the SWS. On the other hand, at the resonant wavelength, the field amplitudes in the resist and the lower TiO_2 are out-of-phase at the SWS-glass interface, and the transmitted field amplitude becomes lower than that at non-resonant wavelength, as shown in Fig. 4(b). These distributions can well explain the origin of the peaks in the reflection spectra of our samples. The

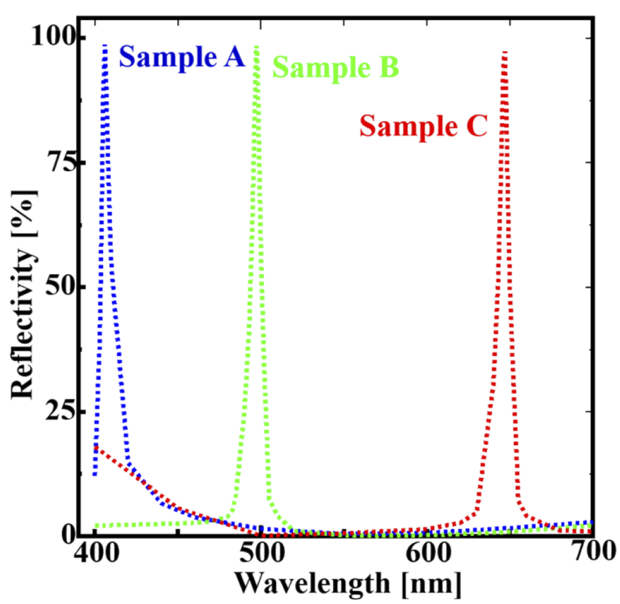

Fig. 3. Calculated reflection spectra of the samples A, B, and C for p-polarization.

Optical Materials EXPRESS

calculation results indicate that various colors can be generated with a high efficiency using our designed structures.

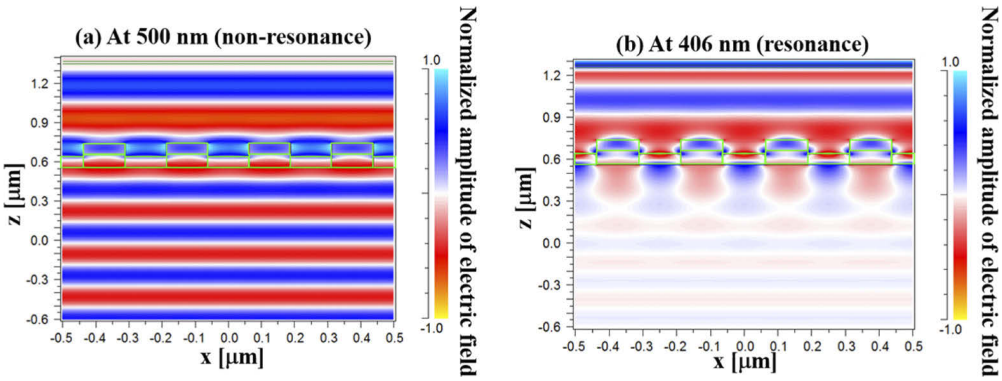

Fig. 4. Calculated electric field distribution of sample A for p-polarized light (a) at non-resonance (500 nm) and (b) at resonance (406 nm) wavelengths.

3. Experimental results and discussion

To experimentally demonstrate the generation of various colors, we fabricated three samples with different structural dimensions. The designed structures were fabricated on a glass substrate. ZEP-520A was spin-coated onto the glass substrates, and its thickness was fixed to 100 nm. The SWS patterns were formed onto 300 × 300 μm square areas using EB lithography. After that, the TiO_2 was EB-evaporated onto the patterned samples with a chamber pressure of 3.2×10^{-4} Pa. The evaporation rate was approximately 0.5–0.6 Å/s. Figure 5 shows the scanning electron microscope (SEM) images of the samples titled at 70°. To produce clear cross sections of the fabricated structures, the edges of the samples were processed by focused ion beam irradiation. The SEM images indicate that the evaporated upper TiO_2 has a rounded shape, and the shape of the lower TiO_2 is almost triangular. The cylindrical shapes of the upper TiO_2 have higher thicknesses and larger widths compared with those in the design. The triangular shapes of the lower TiO_2 result in a higher TiO_2 thickness while the widths decrease.

We measured the reflection spectra under normal incident geometry. A halogen lamp was selected as the white light source to investigate the reflection characteristics of the samples. The light from the halogen lamp was p-polarized by the polarizer placed on the front of the lamp. The emissions from the lamp were entered normally into the SWS using an objective lens (magnification: ×20, NA: 0.4), and the reflected light was focused into the optical fiber connected to the spectrometer (OP-Flame-S Package: Ocean Photonics Co.). Figure 6 shows the measured (solid lines) and calculated (dashed lines) reflection spectra of each fabricated sample. The experimental reflectivity of the samples was calibrated using the reference aluminum mirror (TFA-50C08-4: Sigma Co.). As shown in Fig. 6, the fabricated samples have resonant reflection peaks at different wavelengths. The peak wavelengths depend on the structural parameters of the SWS. Reflection peaks around 413 nm, 510 nm, and 674 nm wavelengths were obtained. As a result, various colors, including R, G, and B, could be generated. The trends of the experimental spectra agree with those of the calculated spectra. The peak reflectivity of each sample also reached approximately 72% (413 nm), 63% (510 nm), and 57% (674 nm). We also evaluated the color purity of the measured spectra using the International Commission on Illumination (CIE) 1931 color matching functions. Figure 7 shows the color pattern of the fabricated samples (400~700 nm wavelength range) in the CIE 1931 chromaticity diagram, and the color patterns are almost comparable to typical structural colors [25]. Our experimental results also show that the

Optical Materials EXPRESS

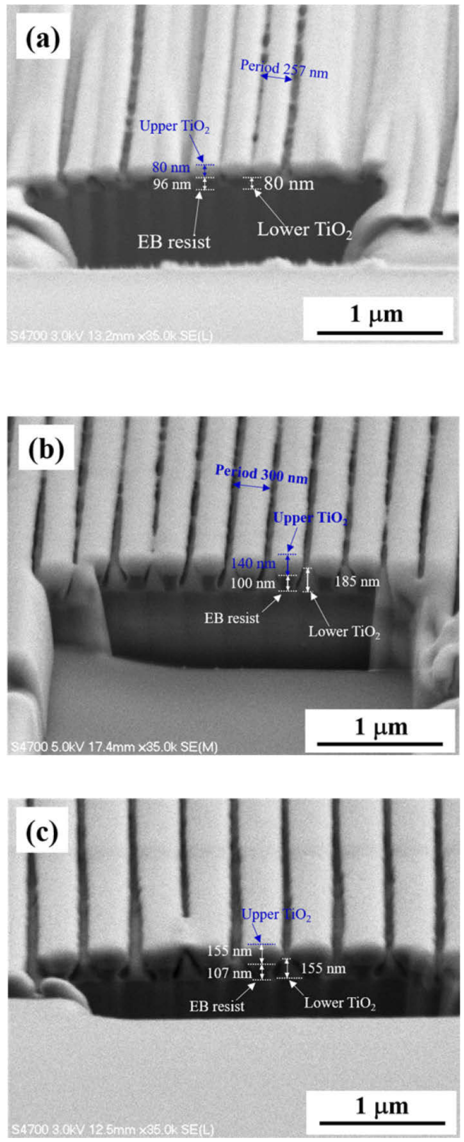

Fig. 5. SEM images of the fabricated samples with different dimensions of SWSs. (a) Sample A, (b) sample B, and (c) sample C. The scale bars represent 1 μm. The areas of the SWSs are 300×300 μm^2.

Optical Materials EXPRESS

reflectivity of our filters, namely efficiency, is higher than that reported in other studies [2,4,6], and is sufficient for the filter to be used in various applications. These results show that our filters successfully achieved various visible colorations with high efficiency. Moreover, our filters can be manufactured without the lift-off and etching processes that other filters require. This vastly improves the potential manufacturing throughput of our color filters.

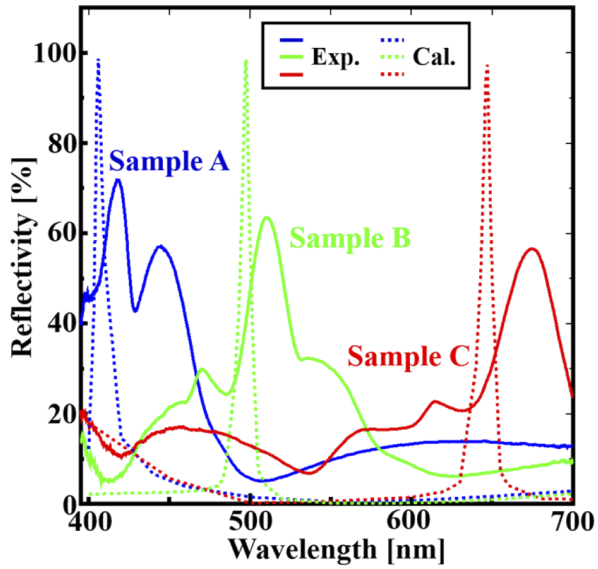

Fig. 6. Reflection spectra of the fabricated samples for p-polarization. The solid and the dashed lines are the experimental and the FDTD calculated spectra, respectively.

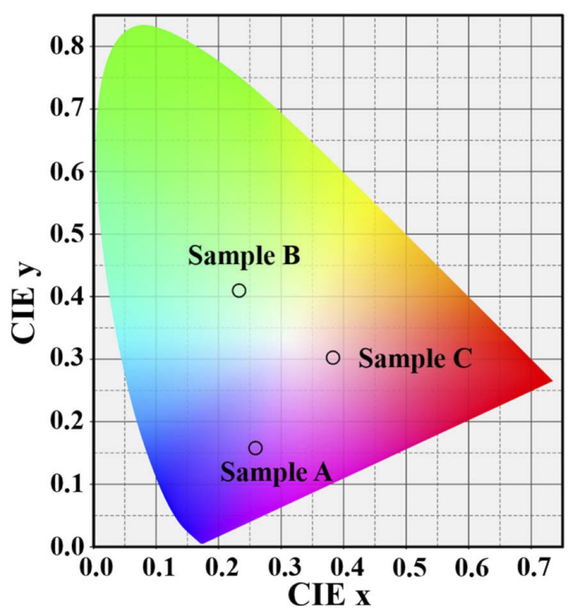

Fig. 7. Color pattern of the fabricated samples in the CIE 1931 chromaticity diagram.

Optical Materials EXPRESS

On the other hand, there are deviations between the experimental and FDTD calculated reflection spectra. The peak wavelengths of each fabricated sample are red-shifted and the peak reflectivities are lower compared with the calculated results. Moreover, several unpredicted peaks are observed in the measured spectra. In particular, sample A shows two clear blue peaks. We believe that the deviations between the experiments and calculations may be a result of the imperfect shapes of the fabricated SWSs.

As shown in the SEM images of the samples (Fig. 5), the evaporated TiO_2 structures do not have an ideal rectangular shape. The upper TiO_2 shapes are slightly rounded and the lower are triangular. These imperfections lead to fluctuations in the periodic RI distribution of our SWSs. These fluctuations have a large effect on the mode phases and amplitudes, which define the reflection properties of the SWSs [26,27]. Thus, the measured spectra deviate from the FDTD calculations. This suggests that the suppression of fabrication imperfections and control of the shape of the SWSs contribute to more precise color control and higher efficiency. Optimizing the shape control of double-layer SWSs will be the subject of future work.

In addition, the angular dependences of the samples are shown in Fig. 8. The incident angle φ is defined by the tilt from the z-direction in the y-z incident plane (see inset in Fig. 8(a)). Figure 8 indicates that the reflection spectra of the samples are highly sensitive to φ. For example, the peak reflectivities tend to weaken with an oblique incidence and the splitting of some peaks occurs. This angular dependence can be explained as follows. The oblique incidence provides

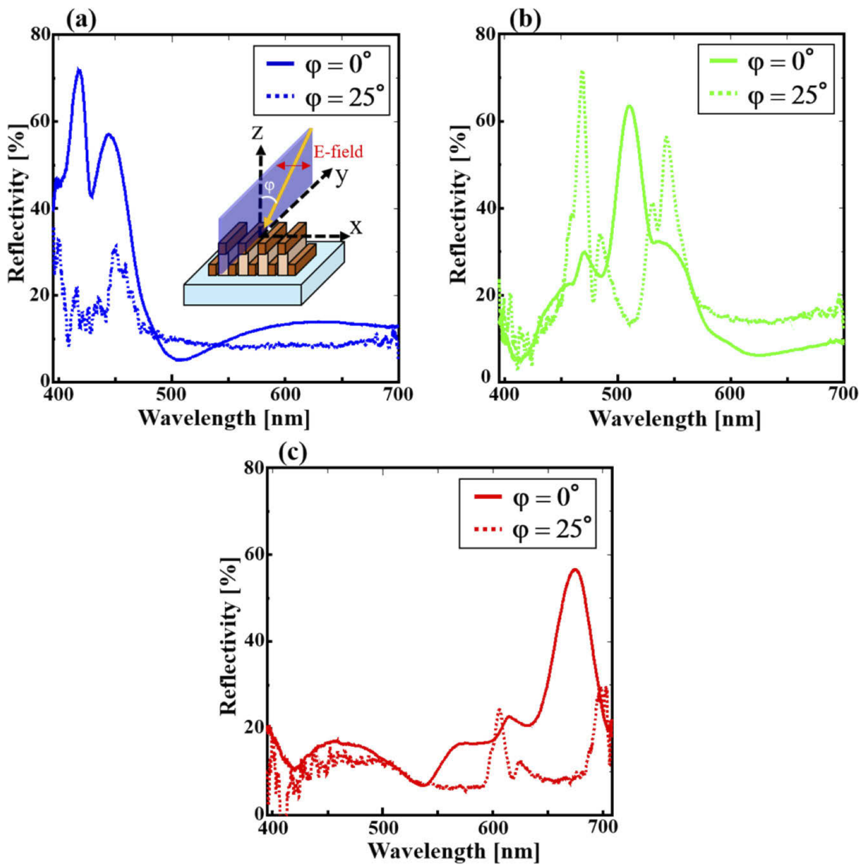

Fig. 8. Incident angle (φ) dependence of the reflection spectra of (a) sample A, (b) sample B, and (c) sample C. The solid and dotted lines indicate φ = 0° and φ = 25°, respectively.

Optical Materials EXPRESS

the lateral wavenumber of light, and this significantly modifies the mode excitation conditions [19]. Hence, the reflection spectra differ from that with normal incidence. These results suggest that our structural colorations possess a narrow viewing angle, and this is very useful for some applications, such as peeping prevention features.

4. Conclusion

In conclusion, highly reflective color filters were experimentally demonstrated. Depending on the structural parameters of the double-layers SWS fabricated on the glass substrate, their reflection spectra showed various colorations including R, G, and B, with high efficiency (57%, 63%, and 72%). Moreover, these filters can be manufactured without the nano-pattern lift-off and etching processes, which will contribute to a significant improvement in their manufacturing throughput.

Funding. Japan Society for the Promotion of Science (JP18K04238, JP21K14515).

Acknowledgments. The authors thank C. Azuma of Tokushima University for technical support in SEM measurements. This work was partially supported by JSPS KAKENHI Grant Number JP18K04238 and JP21K14515.
All authors contributed equally to this work.

Disclosures. The authors declare no conflicts of interest.

Data availability. Data underlying the results presented in this paper are not publicly available at this time but may be obtained from the authors upon reasonable request.

References

1. Y. Gu, L. Zhang, J. K. Yang, S. P. Yeo, and C. W. Qiu, "Color generation via subwavelength plasmonic nanostructures," Nanoscale **7**(15), 6409–6419 (2015).
2. Z. Li, A. W. Clark, and J. M. Cooper, "Dual color plasmonic pixels create a polarization controlled nano color palette," ACS Nano **10**(1), 492–498 (2016).
3. D. Fleischman, K. T. Fountaine, C. R. Bukowsky, G. Tagliabue, L. A. Sweatlock, and H. A. Atwater, "High spectral resolution plasmonic color filters with subwavelength dimensions," ACS Photonics **6**(2), 332–338 (2019).
4. R. Mudachathi and T. Tanaka, "Up scalable full colour plasmonic pixels with controllable hue, brightness and saturation," Sci. Rep. **7**(1), 1199 (2017).
5. Y. Ma, N. Sun, R. Zhang, L. Guo, Y. She, J. Zheng, and Z. Ye, "Integrated color filter and polarizer based on two-dimensional superimposed nanowire arrays," J. Appl. Phys. **116**(4), 044314 (2014).
6. Y. Lee, J. Yun, M. Seo, S. J. Kim, J. Oh, C. M. Kang, H. J. Sun, T. D. Chung, and B. Lee, "Full-color-tunable nanophotonic device using electrochromic tungsten trioxide thin film," Nano Lett. **20**(8), 6084–6090 (2020).
7. N. Fang, H. Lee, C. Sun, and X. Zhang, "Sub–diffraction-limited optical imaging with a silver superlens," Science **308**(5721), 534–537 (2005).
8. Y. T. Yoon, C. H. Park, and S. S. Lee, "Highly efficient color filter incorporating a thin metal–dielectric resonant structure," Appl. Phys. Express **5**(2), 022501 (2012).
9. Y. Jung, H. Jung, H. Choi, and H. Lee, "Polarization selective color filter based on plasmonic nanograting embedded etalon structures," Nano Lett. **20**(9), 6344–6350 (2020).
10. S. Sun, Z. Zhou, C. Zhang, Y. Gao, Z. Duan, S. Xiao, and Q. Song, "All-dielectric full-color printing with TiO_2 metasurfaces," ACS Nano **11**(5), 4445–4452 (2017).
11. Y. Nagasaki, M. Suzuki, and J. Takahara, "All-dielectric dual-color pixel with subwavelength resolution," Nano Lett. **17**(12), 7500–7506 (2017).
12. J. Proust, F. Bedu, B. Gallas, I. Ozerov, and N. Bonod, "All-dielectric colored metasurfaces with silicon Mie resonators," ACS Nano **10**(8), 7761–7767 (2016).
13. I. Koirala, S. S. Lee, and D. Y. Choi, "Highly transmissive subtractive color filters based on an all-dielectric metasurface incorporating TiO_2 nanopillars," Opt. Express **26**(14), 18320–18330 (2018).
14. W. Yang, S. Xiao, Q. Song, Y. Liu, Y. Wu, S. Wang, J. Yu, J. Han, and D. P. Tsai, "All-dielectric metasurface for high-performance structural color," Nat. Commun. **11**(1), 1–8 (2020).
15. M. J. Uddin and R. Magnusson, "Highly efficient color filter array using resonant Si_3N_4 gratings," Opt. Express **21**(10), 12495–12506 (2013).
16. L. Zhu, J. Kapraun, J. Ferrara, and C. J. Chang-Hasnain, "Flexible photonic metastructures for tunable coloration," Optica **2**(3), 255–258 (2015).
17. V. Vashistha, G. Vaidya, R. S. Hegde, A. E. Serebryannikov, N. Bonod, and M. Krawczyk, "All-dielectric metasurfaces based on cross-shaped resonators for color pixels with extended gamut," ACS Photon. **4**(5), 1076–1082 (2017).
18. C. J. Chang-Hasnain, "High-contrast gratings as a new platform for integrated optoelectronics," Semiconductor Sci. Tech. **26**(1), 014043 (2011).
19. C. J. Chang-Hasnain and W. Yang, "High-contrast gratings for integrated optoelectronics," Adv. Opt. Photon. **4**(3), 379–440 (2012).

Optical Materials EXPRESS

20. V. Karagodsky, F. G. Sedgwick, and C. J. Chang-Hasnain, "Theoretical analysis of subwavelength high contrast grating reflectors," Opt. Express **18**(16), 16973–16988 (2010).
21. H. Kikuta, H. Toyota, and W. Yu, "Optical elements with subwavelength structured surfaces," Opt. Rev. **10**(2), 63–73 (2003).
22. L. Qian, D. Zhang, B. Dai, Q. Wang, Y. Huang, and S. Zhuang, "Optical notch filter with tunable bandwidth based on guided-mode resonant polarization-sensitive spectral feature," Opt. Express **23**(14), 18300–18309 (2015).
23. M. J. Uddin, T. Khaleque, and R. Magnusson, "Guided-mode resonant polarization-controlled tunable color filters," Opt. Express **22**(10), 12307–12315 (2014).
24. S. Sarkar, V. Gupta, M. Kumar, J. Schubert, P. T. Probst, J. Joseph, and T. A. König, "Hybridized guided-mode resonances via colloidal plasmonic self-assembled grating," ACS Appl. Mater. Interfaces **11**(14), 13752–13760 (2019).
25. W. Yue, S. Gao, S.-S. Lee, E.-S. Kim, and D.-Y. Choi, "Highly reflective subtractive color filters capitalizing on a silicon metasurface integrated with nanostructured aluminum mirrors," Laser Photonics Rev. **11**(3), 1600285 (2017).
26. Y. Takashima, R. Shimizu, M. Haraguchi, and Y. Naoi, "Influence of low-contrast subwavelength grating shape on polarization characteristics of GaN-based light-emitting diode emissions," Opt. Eng. **54**(6), 067112 (2015).
27. G. Sridharan and S. Bhattacharya, "Simplified analysis of sub-wavelength triangular gratings by simplified modal method," Appl. Phys. **55**(34), 9712 (2016).